Biomaterials 67 (2015) 323–334

Contents lists available at ScienceDirect

Biomaterials

journal homepage: www.elsevier.com/locate/biomaterials

Persistent luminescence nanoprobe for biosensing and lifetime imaging of cell apoptosis via time-resolved fluorescence resonance energy transfer

Lei Zhang, Jianping Lei*, Jintong Liu, Fengjiao Ma, Huangxian Ju**

State Key Laboratory of Analytical Chemistry for Life Science, School of Chemistry and Chemical Engineering, Nanjing University, Nanjing 210093, PR China

ARTICLE INFO

Article history:
Received 4 April 2015
Received in revised form
17 July 2015
Accepted 20 July 2015
Available online 21 July 2015

Keywords:
Biosensor
Fluorescent probe
Caspase
Image analysis
Persistent luminescence nanoparticles

ABSTRACT

Time-resolved fluorescence technique can reduce the short-lived background luminescence and auto-fluorescence interference from cells and tissues by exerting the delay time between pulsed excitation light and signal acquisition. Here, we prepared persistent luminescence nanoparticles (PLNPs) to design a universal time-resolved fluorescence resonance energy transfer (TR-FRET) platform for biosensing, lifetime imaging of cell apoptosis and *in situ* lifetime quantification of intracellular caspase-3. Three kinds of PLNPs-based nanoprobes are assembled by covalently binding dye-labeled peptides or DNA to carboxyl-functionalized PLNPs for the efficient detection of caspase-3, microRNA and protein. The peptides-functionalized nanoprobe is also employed for fluorescence lifetime imaging to monitor cell apoptosis, which shows a dependence of cellular fluorescence lifetime on caspase-3 activity and thus leads to an *in situ* quantification method. This work provides a proof-of-concept for PLNPs-based TR-FRET analysis and demonstrates its potential in exploring dynamical information of life process.

1. Introduction

Time-resolved fluorescence (TRF), which can reduce the short-lived background luminescence and auto-fluorescence interference from cells and tissues by exerting the delay time between pulsed excitation light and signal acquisition, provides a background-free approach in life science [1–3]. In particular, coupling with the advantage of fluorescence resonance energy transfer (FRET), the time-resolved fluorescence resonance energy transfer (TR-FRET) assay offers high sensitivity in comparison with conventional FRET [4]. TR-FRET assays have been extensively applied in detection and imaging of biomolecules by employing organic fluorophores [5], fluorescent proteins [6,7], polymer materials [8], and nanoparticles as luminescent probes [9–17]. However, most of the reported TRF probes suffer from the vulnerability to environmental media, and the interference of multi-emission peaks, thus limit their further applications.

Persistent luminescence nanoparticles (PLNPs, also called long-lasting afterglow nanoparticles) can store the excitation energy and then slowly release it by a photonic emission [18–20]. The persistent luminescence can last several hours after removal of excitation resource, providing many conveniences in optical assay and imaging [21–23]. Scherman's group pioneered a series of applications of near-infrared PLNPs in real-time optical imaging of small animals without the need of any external illumination source [24–27]. Recently, several PLNPs probes have been developed for biosensing based on their inhibition of FRET or electron transfer to the quencher [28–31]. However, the attempt to employ PLNPs for TR-FRET analysis and lifetime imaging has not been made yet. Obviously, the energy transfer from the afterglow of PLNPs to short-lived organic dyes can apparently lengthen the fluorescence lifetime of acceptors, which greatly meets the TRF requirement. Thus PLNPs as a class of long-lifetime probes are very powerful for TR-FRET biosensing and time-resolved lifetime imaging of cellular biomolecules without background interference.

Here, we synthesized PLNPs probes of highly efficient persistent luminescence to design a universal TR-FRET platform for biosensing by setting appropriate delay time and gate time (Scheme 1a). The luminescence of fluorescein isothiocyanate (FITC) is effectively suppressed due to its shorter lifetime than delay time, which represents an interval between pulsed excitation light and signal acquisition. The long-lived luminescence of PLNPs is

* Corresponding author.
** Corresponding author.
E-mail addresses: jpl@nju.edu.cn (J. Lei), hxju@nju.edu.cn (H. Ju).

http://dx.doi.org/10.1016/j.biomaterials.2015.07.037
0142-9612/

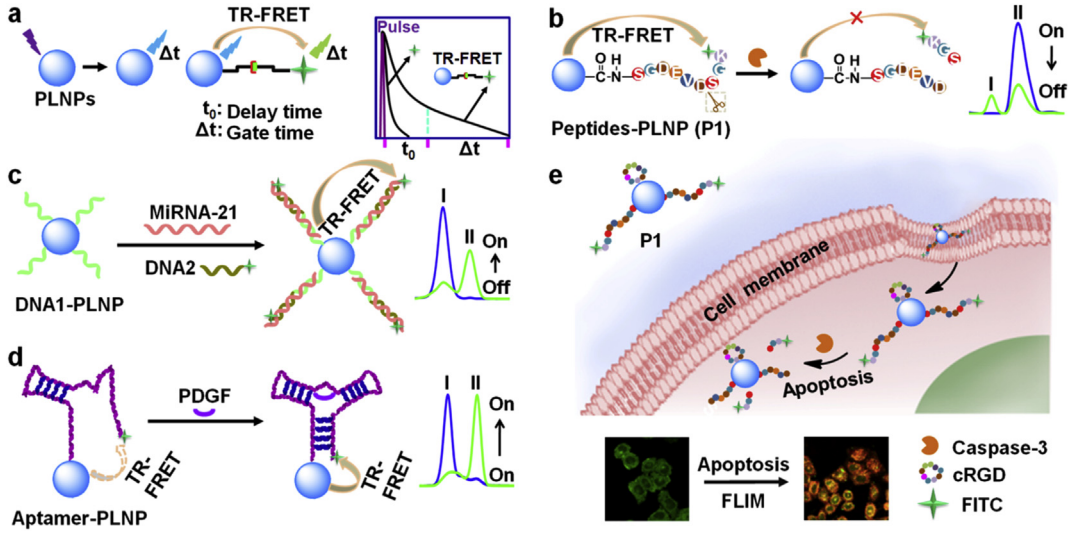

Scheme 1. Schematic illustration for (a) PLNPs-based TR-FRET principle, (b–d) TR-FRET detection strategies of caspase-3 protease, miRNA-21 and PDGF protein by using caspase-specific peptide & cRGD-, DNA1-and aptamer-functionalized PLNPs probes, respectively, and (e) lifetime imaging of intracellular caspase-3 activity using **P1** during cell apoptosis by FLIM. I and II represent TRF signals of PLNPs donor at 468 nm and FITC acceptor at 520 nm, respectively. Blue and green lines represent the TRF curves before and after the response of the corresponding target, respectively.

captured in the gate time designating the time for signal acquisition. Once TR-FRET occurs from PLNPs to FITC, the signal of FITC is acquired in the gate time. Using caspase-3 (related to cell apoptosis) [32–34], microRNA-21 (miRNA-21) and platelet-derived growth factor (PDGF) as the model targets, three recognition nanoprobes are prepared by covalently assembling cyclic arginine–glycine–aspartic acid peptide (cRGD) and FITC-labeled substrate peptide, DNA or aptamer on PLNPs for "on–off", "off–on" and "on–on" TR-FRET detection of enzyme activity, nucleic acids and proteins, respectively. The "on–off" method results from the enzymatic cleavage reaction to release the FITC from the peptide and thus inhibits the FRET from PLNPs to FITC (Scheme 1b). The "off–on" switch is generated by the sandwich hybridization among DNA1, miRNA-21 and DNA2 to achieve the FRET from PLNPs to FITC (Scheme 1c). After the recognition of the FITC-labeled aptamer to target protein, their structure change brings the FITC closer to PLNPs and thus produces an "on–on" TR-FRET strategy (Scheme 1d).

Indeed, many elegant fluorescent probes including graphene oxide–peptide conjugate [35], aggregation light-up tetraphenylethene fluorogen [36], and a genetically encoded fluorescent protein [37], have been developed for detection of caspase activity in live cells [38,39]. However, these proposed methods were usually susceptible to the short-lived auto-fluorescence interference from cells and tissues. Considering that fluorescence lifetime of the probe depends on the recognition to the target, the "on–off" TR-FRET strategy can be further used for lifetime imaging of caspase-3 activity in live cells via fluorescence lifetime imaging microscopy (FLIM) (Scheme 1e), which is an imaging technique based on the differences in the exponential decay rate of the fluorescence from a fluorophore, rather than its intensity [40]. More importantly, this work presents the dependence of cellular lifetime of PLNPs on caspase-3 activity, which produces a novel protocol for *in situ* quantification of caspase-3 activity in single cell based on fluorescence lifetime, and thus provides a robust approach for dynamic evaluation of caspase-dependent cell apoptosis.

2. Materials and methods

2.1. Materials and reagents

Human caspase-3 (active) recombinant protein and cell lysis buffer were purchased from millipore (Billerica, MA, USA). Platelet-derived growth factor (PDGF)-BB was purchased from R&D System (Minneapolis, MN, USA) and was dissolved in 4 mM HCl containing 0.1% BSA. Caspase-3 inhibitor (Ac-DEVD-CHO), caspase-3 fluorogenic assay kit, 3-(4,5-dimethylthiazol-2-yl)-2,5-diphenyltetrazolium bromide (MTT), HeLa cells and Annexin V-FITC/propidium iodide (PI) cell apoptosis kit were purchased from Nanjing Keygen Biotechnology Co. Ltd. (Nanjing, China). DNA hybridization buffer (pH 7.4) contained 10 mM Tris–HCl, 1 mM EDTA, 50 mM NaCl and 10 mM $MgCl_2$. Caspase assay buffer contained 40 mM HEPES (pH 7.4), 100 mM NaCl, 1 mM EDTA, 10% sucrose, 0.1% CHAPS and 10 mM DTT. Phosphate buffer saline (PBS, pH 7.4) contained 136.7 mM NaCl, 2.7 mM KCl, 8.72 mM Na_2HPO_4 and 1.41 mM KH_2PO_4. Human caspase-3 (active) recombinant protein was reconstituted to 1.0 unit μL^{-1} with PBS containing 15% glycerol. All other reagents were of analytical grade. All aqueous solutions were prepared using ultrapure water ($\geq$18 MΩ, Milli-Q, Millipore).

Caspase-3 specific peptide SGDEVDSGK-FITC, control peptide SGDEVGSGK-FITC, cRGD and DNA oligonucleotides were synthesized and purified by Sangon Biological Engineering Technology & Co. Ltd. (Shanghai, China). RNA oligonucleotides were purchased from Shanghai GenePharma Co., Ltd. (Shanghai, China). The DNA and RNA oligonucleotides included:

DNA1, 5′-NH_2 TCA ACA TCA GT-3′; (note: DNA1 was functionalized with FITC at 3′ for FRET parameter measurements.)

DNA2, 5′-NH_2 CTG ATA AGC TA (FITC)-3′;

PDGF-BB aptamer, 5′-NH_2 CAG GCT ACG GCA CGT AGA GCA TCA CCA TGA TCC TG (FITC)-3′;

PDGF-BB control DNA, 5′-NH_2 CAG CGT ACG GCA CGT ACC GAT TCA CCA TGA AGC TG (FITC)-3′;

miRNA-21, UAGCUUAUCAGACUGAUGUUGA;

single-base mismatched miRNA-21, UAGCUUAUCAGACUGAU

GUU***C***A;

two-base mismatched miRNA-21, UAGCUUAUCAGAC***A***GAUG UU***C***A;

three-base mismatched miRNA-21, UA***A***CUUAUCAGAC***A***GAUG UU***C***A.

The underlined and italic letters represent the mismatched base.

2.2. Synthesis of PLNPs

The PLNPs were synthesized with a sol–gel approach [24]. Raw materials included strontium nitrate ($Sr(NO_3)_2$), zinc nitrate hexahydrate ($Zn(NO_3)_2{\cdot}6H_2O$), magnesium nitrate hexahydrate ($Mg(NO_3)_2{\cdot}6H_2O$), europium nitrate pentahydrate ($Eu(NO_3)_3{\cdot}5H_2O$) and dysprosium nitrate pentahydrate ($Dy(NO_3)_3{\cdot}5H_2O$). These salts were dissolved in water with the concentrations of 0.1 M. 4.5 mL of $Sr(NO_3)_2$, 1.0 mL of $Mg(NO_3)_2$, 2.5 mL of $Zn(NO_3)_2$, 0.03 mL of $Eu(NO_3)_3$ and 0.02 mL of $Dy(NO_3)_3$ were mixed as the reaction solution. 2.0 mL of tetraethyl orthosilicate (TEOS) was then added rapidly in the mixture to heat at 70 °C until the sol-to-gel transition occurred. The wet gel was dried in an oven at 110 °C for 20 h, and then directly dried in a zircone crucible in a weak reductive atmosphere (5% H_2, 95% Ar) at 1050 °C for 10 h. The resulting powder was ground with an agate mortar and pestle to obtain the fine powder of PLNPs, which was then dispersed by sonication overnight in 25 mL of NaOH (5 mM) to get hydroxylated PLNPs (PLNPs-OH) dispersion. The PLNPs with nanosized diameter were selected according to the centrifugation method [25].

2.3. Functionalization of PLNPs

The amino-functionalized persistent luminescence nanoparticles (PLNPs-NH_2) and carboxyl-functionalized PLNPs (PLNPs-COOH) were synthesized according to a previously reported protocol (Scheme 2) [41,42]. PLNPs-NH_2 was obtained by adding 100 μL of APTES to 10 mL of PLNPs-OH (2.0 mg mL^{-1} in DMF) and stirring overnight at 80 °C. The resulting nanoparticles were centrifuged and washed with DMF for three times to remove the excess APTES. To obtain PLNPs-COOH, 11.6 mg of diglycolic anhydride was added in 2 mL of PLNPs-NH_2 dispersion (2.5 mg mL^{-1} in DMF) and stirred overnight. These surface functionalized PLNPs were dispersed in water for further experiments.

2.4. Preparation of peptide functionalized PLNPs

First of all, the carboxyl groups on PLNPs-COOH (25 mg) were pre-activated with EDC (10 mg) and Sulfo-NHS (20 mg) in MES buffer (5 mL, 100 mM, pH 5.6) for 40 min. After centrifugation, the supernatant was removed, and 5 mL of the mixture of cRGD peptide (0.25 mM) and caspase-specific or nonspecific peptide (1 mM) was added to react with the activated PLNPs. Then the mixture was adjusted to pH 8 with 1 M NaOH and stirred in dark at room temperature for 8 h. The unreacted peptide was removed by centrifugation. The resulting caspase-specific peptide & cRGD-PLNPs (**P1**) and caspase-nonspecific peptide & cRGD-PLNPs (**P2**) were washed three times with PBS. For preparation of cRGD-PLNPs, 5 mL of the cRGD peptide (1 mM) was added to react with the activated PLNPs-COOH. The peptide functionalized PLNPs were redispersed in PBS for further use.

2.5. Measurements

X-ray powder diffraction (XRD) pattern was recorded using an XRD-6000 diffractometer (Shimadzu Co., Japan), equipped with a rotating anode and a Cu Kα radiation source. The transmission electron microscopic (TEM) image was obtained on a JEM-2100 transmission electron microscope (JEOL Ltd., Japan). Dynamic light scattering (DLS) was observed on a 90 Plus/BI-MAS equipment (Brook haven, USA). Zeta potential analysis was performed on a Zetasizer (Nano-Z, Malvern, UK). Fourier transform infrared (FT-IR) spectra were recorded on a Nicolet NEXUS870 spectrometer (Madison, WI). Thermal gravimetric analyzer (TGA) experiments were performed on a TGA-DSC 1 thermal analyzer (Mettler-Toledo) under pure N_2 in the range from 20 to 800 °C with a heating rate of 10 °C min^{-1}. The UV–vis absorption spectra were obtained with a UV-3600 UV–Vis–NIR spectrophotometer (Shimadzu Co., Kyoto, Japan) and Nanodrop-2000C (Nanodrop, USA). The fluorescence spectra were obtained on an RF-5301PC spectrofluorophotometer (Shimadzu, Japan). The time-resolved fluorescence (TRF) and caspase-3 fluorescent assay kit experiments were carried out on a Synergy hybrid 1 multimode microplate reader (BioTek). Phosphorescence spectrum and photoluminescence (PL) decay curves were determined on an FLS920 spectrometer (Edinburgh, UK). Flow cytometric analysis was performed on a Coulter FC-500 flow cytometer (Beckman-Coulter). The cell confocal images were gained on a TCS SP5 laser scanning confocal microscope (Leica, Germany). MTT assay was performed on a microplate reader (680, Bio-Rad, USA).

2.6. TRF assay

100 μL of the mixture of **P1** (1.0 mg mL^{-1}) and caspase-3 sample or recombinant caspase-3 at different concentrations in caspase assay buffer was added to each well. As control, caspase-3 inhibitor (100 μM) was added to the mixture. After the plate was incubated at 37 °C for 2 h, the wells were excited at 365 nm for 10 min, and the TRF spectra were directly measured on a microplate reader by scanning from 400 to 600 nm with an interval of 10 nm, where the delay time and gate time (if not specifically explained) were set to be 50 μs and 1000 μs, respectively. For detection of miRNA-21 and PDGF, the incubation time was 2 and 1 h, respectively.

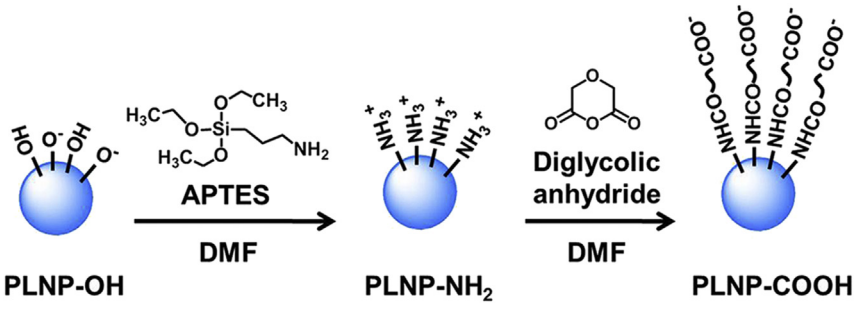

Scheme 2. Schematic representation of PLNP surface modification of –OH, $-NH_2$ and –COOH.

2.7. FRET parameters measurements

The experimental FRET efficiency E is defined as Eq. (1) [43]:

$$E = \frac{(F_D - F_{DA})}{F_D} \quad (1)$$

where F_D and F_{DA} are the fluorescence intensity of the donor (PLNP) alone and the donor in the presence of acceptor (FITC dye), respectively.

Förster distance R_0 designating the donor–acceptor separation at 50% energy transfer efficiency is expressed as Eq. (2) [44]:

$$R_0 = 9.78 \times 10^3 \left[k^2 n_D^{-4} \Phi_D J(\lambda)\right]^{1/6} \quad (2)$$

where n_D is the refractive index of the medium, Φ_D is the donor quantum yield in the absence of acceptor, J (λ) is the spectral overlap integral, and κ^2 is the dipole orientation factor. Here, J (λ) value was obtained through origin 8.5 software, the Φ_D value was calculated according to the following Eq. (3) [45]:

$$\Phi_D = \Phi_s \times \frac{A_s}{A_x} \times \frac{F_x}{F_s} \times \left(\frac{n_x}{n_s}\right)^2 \quad (3)$$

where A is the absorbance, F is the area under the emission curve, n is the refractive index of the solvent used in the measurement, and the subscripts s and x represent the standard and sample, respectively. Here, quinine sulfate was used as the standard.

Estimate of the PLNP donor–dye acceptor separation distance (r) is calculated using the Eq. (4) [46]:

$$r = \left(\frac{n(1-E)}{E}\right)^{1/6} R_0 \quad (4)$$

where n is the number of dye acceptors attached to the PLNPs donor.

2.8. Cell culture

HeLa cells were cultured in a flask in Dulbecco's modified Eagle's medium (DMEM, Gibco) supplemented with 10% fetal calf serum (FCS, Gibco), penicillin (100 μg mL^{-1}), and streptomycin (100 μg mL^{-1}) at 37 °C in a humidified atmosphere containing 5% CO_2. Cell number was determined using a Petroff-Hausser cell counter (USA).

2.9. Caspase-3 activity assay in cell extract

HeLa cells treated with apoptosis inducer (cisplatin) for 3 h were collected in the exponential phase of growth, and 1.0×10^6 cells were dispensed in a 1.5-mL Ependorff tube, washed twice with ice-cold PBS (0.1 M, pH 7.4), and resuspended in 200 μL of ice-cold caspase lysis buffer containing pH 7.4 HEPES-NaOH, 0.1% sucrose, 1% CHAPS, 2 mM EDTA and 10 mM DTT. The mixture was incubated for 30 min on ice and centrifuged at 10,000 rpm for 5 min. The supernatant was collected as cell extract for caspase-3 analysis. As the control, caspase-3 inhibitor was incubated with HeLa cells for 6 h before treated with apoptosis inducer.

Caspase-3 activity in cell extract was then measured using a caspase-3 fluorogenic assay kit. Briefly, 30 μL of the extracts from apoptosis inducer-treated cells were mixed with 60 μL of caspase assay buffer and 10 μL substrate probe from the kit. After incubation at 37 °C for 2 h, the fluorescent product was detected with a multimode microplate reader at 485 nm excitation and 535 nm emission.

2.10. Cytotoxicity evaluation

The cytotoxicity of **P1** was examined by MTT assay. Briefly, after HeLa cells (100 μL, 5.0×10^5) were seeded in the wells of 96-well plate for 12 h, the medium was discarded. The cells were then washed twice with PBS, and incubated with 100 μL culture medium containing 20 μL **P1** (1.0 mg mL^{-1}) for different times. Meanwhile, the cells were incubated with 100 μL culture medium without **P1** as control. After incubated with MTT for 4 h at 37 °C, the absorbance of the cells was measured using microplate reader at 490 nm. The relative cell viability (%) was calculated by $(A_{test}/A_{control}) \times 100$.

2.11. Confocal fluorescence imaging

HeLa cells were seeded into 35-mm confocal dishes (Glass Bottom Dish) at a density of 5.0×10^4 per dish and incubated for 12 h at 37 °C. The medium was then replaced with fresh culture medium containing 1.0 mg mL^{-1} **P1** and incubated for 4 h. The fluorescence of cells was visualized with a confocal laser scanning microscope at stationary parameters including the laser intensity, exposure time and objective lens. Prior to imaging, the cells were rinsed three times with PBS and kept in PBS. The cells were excited at 405 nm with a diode laser and the emission was collected from 450 to 495 nm. All images were digitized and analyzed with Leica Application Suite Advanced Fluorescence (LAS-AF) software package.

2.12. Cell apoptosis experiments

Briefly, 5.0×10^5 HeLa cells per well were seeded for 12 h in a 6-well plate containing 1.5 mL fresh DMEM in each well. These cells were then incubated with cell apoptosis inducer for different times. The resulting cells were collected, stained with the mixture of 5.0 μL Annexin V-FITC and 5.0 μL PI for 15 min, and analyzed with flow cytometry over FL1 (Annexin V-FITC) and FL3 (PI) channels.

2.13. FLIM experiments

5.0×10^4 HeLa cells in 35-mm confocal dishes were incubated with **P1** or **P2** (1.0 mg mL^{-1}) for 4 h at 37 °C. After treatment with apoptosis inducer for the designed time, the FLIM images of HeLa cells were carried out on an Olympus IX81 laser scanning microscope integrated with FLIM setup. The fluorescence signal was detected by the system of the confocal microscope, and correlative calculation of the data was performed with professional software which was provided by PicoQuant Company. The light from the pulse diode laser head (PicoQuant, PDL 800-D) with excitation wavelength of 405 nm was focused onto the sample with a 40×/NA 0.95 objective lens. The emitted fluorescence signal was collected at 450–495 nm.

2.14. Quantification of intracellular caspase-3

HeLa cells (5.0×10^4) were first incubated with **P1** (1.0 mg mL^{-1}) for 4 h, and then treated with apoptosis inducer at concentrations from 12.5 to 100 μM for 3 h. After washed with PBS three times, these cells were conducted for FLIM experiments to obtain the lifetimes from the software of FLIM setup. The corresponding caspase-3 concentrations of the treated HeLa cells were then detected via *in vitro* caspase-3 kit analysis of the cell extracts using a standard curve of fluorescence intensity *vs.* logarithmic value of caspase-3 concentration (C). The obtained C values were then used for obtaining the calibration curve for quantification of intracellular caspase-3 concentration in single cell by detecting the

lifetime (τ). The plot of τ *vs.* Log *C* in single cell followed a linear regression equation of $\tau = 2869.5 + 246.58 \times \text{Log } C$.

3. Results and discussion

3.1. Characterization and optical properties of PLNPs

The actual composition determined by X-ray fluorescence spectrometry included the matrix $Sr_{1.6}Mg_{0.3}Zn_{1.1}Si_2O_7$ and doped luminescent ions Eu^{2+} and Dy^{3+}. The XRD pattern of this material indicated an orthorhombic system (Fig. 1a). After size selection with a centrifugation method, DLS analysis showed an average hydrodynamic diameter of ~95.5 nm, which was close to the size of 90 ± 10 nm observed from TEM image (Fig. 1b). The synthesized PLNPs had phosphorescent property as most silicate persistent luminescence material (Fig. 1c). Photoluminescence afterglow after irradiation with UV lamp showed a typical characteristic of PLNPs, which can kept stable for at least 10 h without excitation *in situ* (Fig. 1d). By using a CCD camera, the persistent luminescence was detectable for ~16 h (Fig. S1 in Supporting Information).

The fluorescence emission of the synthesized PLNPs occurred at 468 nm under excitation at 365 nm (Fig. 1e), which was ascribed to the transition of the excited state ($4f^65d^1$) to the ground state ($4f^7$) of Eu^{2+} [47]. What's more, the emission spectrum overlapped greatly with the absorption spectrum of FITC, which enabled TR-FRET between long-lived PLNPs and short-lifetime FITC. As a long-lived luminescent reagent, the prepared PLNPs exhibited strong TRF signal in highly contrast to both short-lived FITC and cyanine (Fig. 1f). The fluorescence quantum yield of the PLNPs was 1.9%, comparable to the reported Cr^{3+}/Pr^{3+} doped zinc gallo-germanate PLNPs [18].

Prior to bio-functionalization, hydroxyl groups were first introduced on the surface of PLNPs. After aminosilanization to form amino-terminated PLNPs (PLNPs-NH_2), the Zeta (ζ) potential of hydroxylated PLNPs (PLNPs-OH) changed from −50.1 to +9.37 mV, while the carboxyl coated nanoparticles (PLNPs-COOH) showed a negative ζ potential (Fig. 2a). The surface modifications of PLNPs with amino, carboxyl, and cRGD were further confirmed by FT-IR spectrometry and TGA (Fig. 2b–c). PLNPs-NH_2 showed a strong absorption band of stretching vibration of O–Si–O at 1104 cm^{-1}, an asymmetric and a symmetric $-CH_2-$ stretching bands at 2927 and 2861 cm^{-1}, and the N–H stretching band at 3430 cm^{-1}, indicating the successful amino functionalization of PLNPs. After diglycolic anhydride activation, the resulting PLNPs-COOH showed a strong absorption band at 1610 cm^{-1} for stretching vibration of $-COO^-$. Both DLS analysis and TEM images displayed nanosized amino or carboxyl coated PLNPs (Fig. S2 in Supporting Information). Upon conjugation of cRGD with PLNPs-COOH, a new strong characteristic band for stretching vibration of –CO–NH– occurred at 1650 cm^{-1}, indicating the formation of cRGD-PLNPs conjugate. Bioconjugation of PLNPs-COOH with cRGD made PLNPs available in long-term targeted cancer-cell imaging for 10 h after removal of excitation resource (Fig. S3 in Supporting Information).

3.2. TR-FRET detection of caspase-3 in vitro

For detection of caspase-3, cRGD and FITC-labeled caspase-specific peptide were co-assembled on PLNPs-COOH as the persistent luminescence nanoprobe (**P1**) according to the typical EDC coupling reaction [48]. The amount of the peptides loaded on PLNP was calculated to be 76.5 and 27.1 mg per gram of PLNP for caspase-specific peptide and cRGD, respectively (Fig. S4 in Supporting Information). **P1** was characterized with ζ potential measurements and FT-IR spectra (Fig. S5a-b in Supporting Information). By setting the appropriate delay time and gate time, the TRF spectrum of **P1** showed the FITC signal at 520 nm and the TRF peak of PLNPs decreased at 468 nm (Fig. S5c in Supporting Information), which demonstrated that TR-FRET occurred from long-lived PLNPs to short-lifetime FITC, defined as "on" state. Upon addition of caspase-3 into **P1**, the TRF intensity of PLNPs at 468 nm (F_{468}) increased, while the TR-FRET intensity of FITC at 520 nm (F_{520}) decreased. Therefore, an increased TRF ratio of F_{468} to F_{520} was observed (Fig. 3a), which was defined as "on–off" switch. As a control, no obvious "on–off" switch was observed in the presence of caspase-3 inhibitor or in the mixture of caspase-3 and caspase-nonspecific peptide & cRGD functionalized PLNPs probe (**P2**). The signal change for **P1** could result from the enzymatic cleavage reaction to release the FITC from the peptide. The corresponding

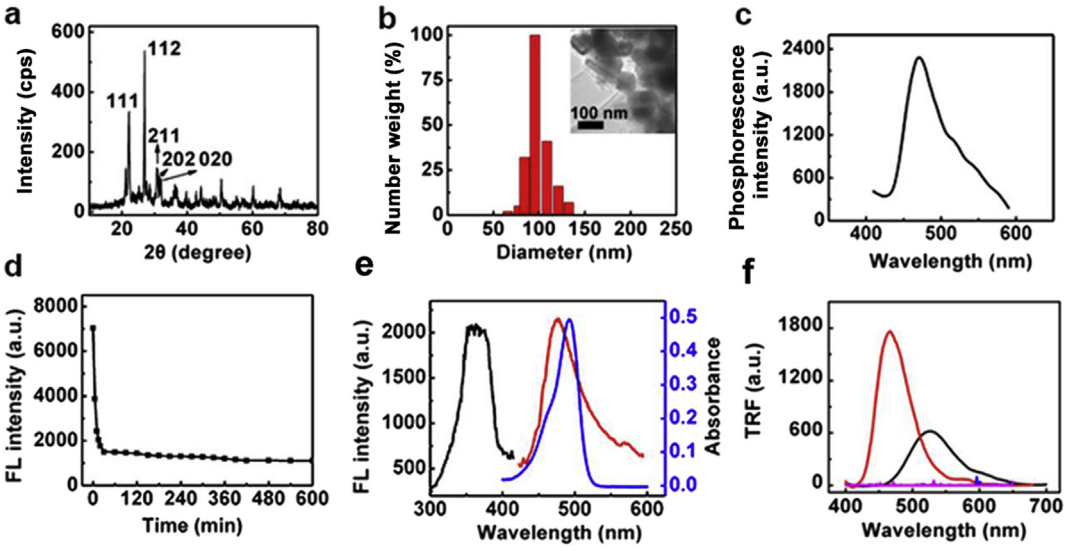

Fig. 1. (a) XRD pattern of PLNPs powder. (b) DLS analysis and TEM image of PLNPs-OH (1.0 mg mL^{-1}). (c) Phosphorescence emission spectrum of PLNPs power. (d) Fluorescence afterglow decay curve of PLNPs power after irradiation with a 365 nm UV. (e) Fluorescence excitation (black), emission (red) spectra of PLNPs and absorption spectrum of FITC (blue, 20 μM). (f) TRF spectra of commercial PLNPs-OH (1.0 mg mL^{-1}, black), synthesized PLNPs-OH (1.0 mg mL^{-1}, red), FITC (1.0 μM, magenta) and cyanine (1.0 μM, blue) with delay time of 100 μs and gate time of 1000 μs. (For interpretation of the references to color in this figure legend, the reader is referred to the web version of this article.)

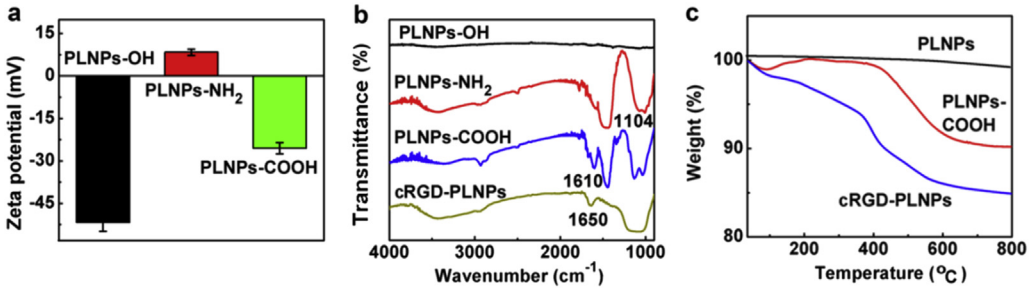

Fig. 2. (a) Zeta (ζ) potential of PLNPs-OH, PLNPs-NH_2 and PLNPs-COOH. Data represent mean values ± standard deviation, $n = 3$. (b) FT-IR spectra of PLNPs-OH, PLNPs-NH_2, PLNPs-COOH and cRGD-PLNPs. (c) TGA curves of unmodified PLNPs, PLNPs-COOH and cRGD-PLNPs.

Michaelis constant K_M (4.9 μM) and turnover number k_{cat} (2.3 s^{-1}) was obtained from the enzymatic kinetic analysis (Fig. 4a). The turnover number was comparable to most fluorescent probes for sensing of caspase-3 activity [49]. The low K_M value indicated the great potential of the developed probe for caspase-3 activity study.

Interestingly, when caspase-3 concentration increased, the PL decay of **P1** at 468 nm was markedly slowed down (Fig. 3b), which indicated that the TR-FRET process from PLNPs to FITC was inhibited. The FRET-induced PL decay of FITC at 520 nm was conversely accelerated with the increasing target concentration (Fig. S6 in Supporting Information), due to the suppression of slow population of its excited state from the excited long-lived PLNPs [12]. The FRET efficiency and PLNPs–FITC separation distance were calculated according to Eqs. (1)–(4) and listed in Table 1. The raised FRET efficiency and the reduced intensity of PLNPs at 468 nm as the increasing peptide concentration (Fig. 4b) identified that the quenching of PLNPs emission resulted from coupling of the FITC-labeled peptides to the PLNPs surface, which brought the FITC acceptor to PLNP donor and produced a non-radiative FRET [50,51].

At the optimized incubation time of 2 h for the enzymatic cleavage reaction between caspase-3 and the substrate peptide on PLNP probes (Fig. 3c), the TRF signal of PLNPs at 468 nm enhanced and TR-FRET peak of FITC at 520 nm decreased with the increasing amount of caspase-3 (Fig. 3d). The concentration of caspase-3 could be quantified by determining the TRF ratio of F_{468} to F_{520} from the calibration curve (inset in Fig. 3d), which showed a detection range from 1.0×10^{-4} to 10 unit mL^{-1} with a detection limit of 2.4×10^{-5} unit mL^{-1} at 3σ. This result was much better than those of an Au–Fe_2O_3 nanoparticles-based fluorescent detection method (0.10–3.0 unit mL^{-1}) and commercial europium(III) chelates-based TRF detection method (0.18–7.1 unit mL^{-1}) [52,53]. For further comparison, the conventional steady-state fluorescence measurements were also conducted, which showed a detection limit of 3.3×10^{-2} unit mL^{-1} under identical conditions (Fig. 3e). Obviously the TR-FRET assay improved the detection sensitivity to a great extent.

To use **P1** for caspase-3 activity detection in practical samples, cell extracts were collected. After HeLa cells were incubated with cisplatin as the apoptosis inducer, a significant change of TRF ratio was observed when **P1** was added in the extract, while the extract of cells pre-incubated with caspase-3 inhibitor showed unobvious change of TRF ratio (Fig. 3f). With the calibration curve, the caspase-

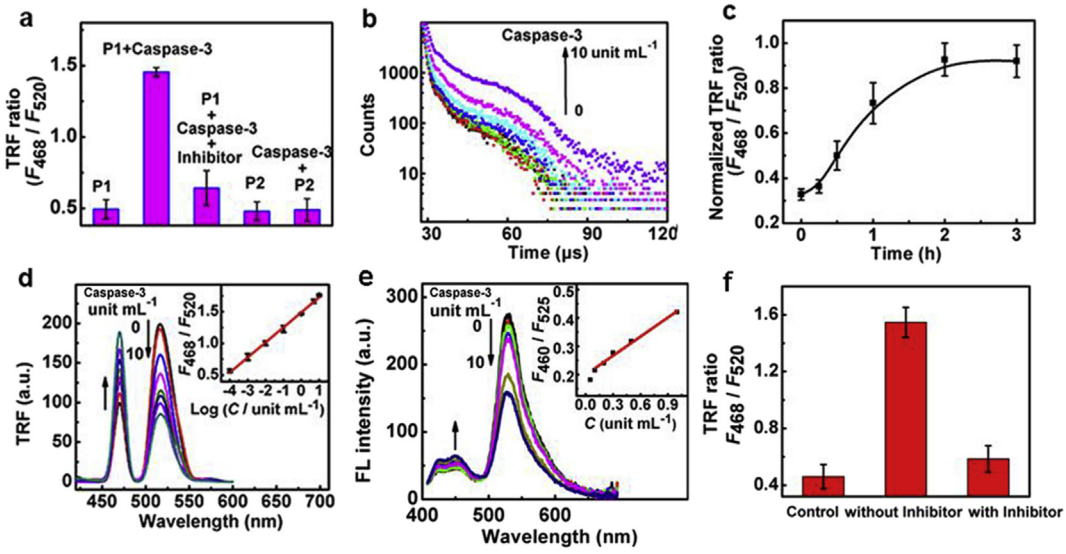

Fig. 3. (a) TRF ratios of F_{468} to F_{520} for **P1** (1.0 mg mL^{-1}), **P1** + caspase-3 (1.0 unit mL^{-1}), **P1** + caspase-3 + caspase-3 inhibitor (100 μM), **P2** (1.0 mg mL^{-1}), and **P2** + caspase-3 (1.0 unit mL^{-1}) in caspase assay buffer. (b) Photoluminescence (PL) decays at 468 nm after incubating **P1** (1.0 mg mL^{-1}) with caspase-3 at 0, 0.0001, 0.001, 0.01, 0.1, 1.0 and 10 unit mL^{-1} (from bottom to top) for 2 h. (c) Optimization of incubation time for the response of **P1** to caspase-3. (d) TRF spectra of **P1** (1.0 mg mL^{-1}) in the presence of 0, 0.0001, 0.001, 0.01, 0.1, 1.0, 5.0 and 10 unit mL^{-1} caspase-3 (from top to bottom at 520 nm). Inset: plot of TRF ratio *vs.* logarithmic value of caspase-3 concentration. (e) Fluorescence spectra of **P1** (1.0 mg mL^{-1}) in the presence of 0, 0.05, 0.1, 0.2, 0.3, 0.5 and 1.0 unit mL^{-1} caspase-3 (from top to bottom at 525 nm). Inset: plot of fluorescence intensity ratio of F_{460} to F_{525} *vs.* caspase-3 concentration. F_{460} and F_{525} represent fluorescence intensity of PLNPs at 460 nm and FITC at 525 nm in steady-state fluorescence spectra, respectively. (f) TRF ratios of **P1** (1.0 mg mL^{-1}) in lysis buffer as control and cell extracts after the cells were treated with and without caspase-3 inhibitor (100 μM) for 6 h and then with cisplatin (100 μM) for 3 h.

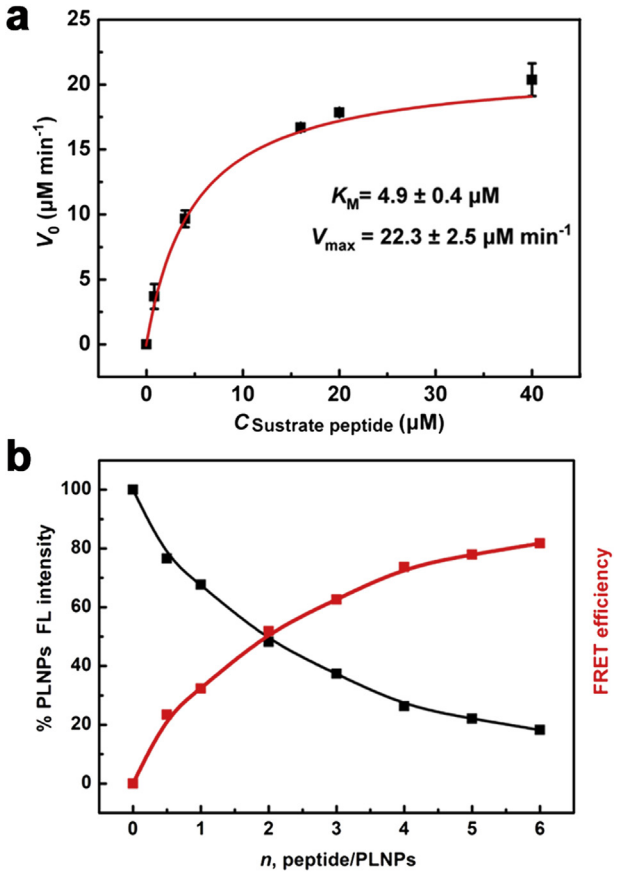

Fig. 4. (a) Caspase enzymatic kinetics assay from a constant amount of caspase-3 (6.7 unit mL^{-1}) with an increasing of substrate concentration. An R^2 = 0.99 was obtained for nonlinear fitting curve. (b) FRET between PLNPs donor and dye acceptor. Plots of fluorescence intensity of PLNPs at 468 nm and the corresponding FRET efficiency *vs*. molar ratio (*n*) of FITC-labeled peptide to PLNPs.

3 concentration in the extract of inducer-treated HeLa cells (1.0×10^6) was 3.8 unit mL^{-1}.

3.3. TR-FRET detection of miRNA-21 and PDGF

MiRNAs, a class of small, non-coding, endogenous RNAs, have essential functions in RNA silencing and post-transcriptional regulation of gene expression, and their expression level is closely related to some major diseases of mankind [54]. For the validation of the universality of PLNPs-based biosensing, an "off—on" TR-FRET sensing strategy was constructed for miRNA detection using DNA-functionalized PLNP as shown in Scheme 1c. The nanoprobe (DNA1-PLNPs) was characterized with UV—vis spectroscopy (Fig. S7a in Supporting Information). The sandwich hybridization among DNA1, FITC-labeled DNA2 and miRNA-21 was validated by polyacrylamide gel electrophoresis in DNA hybridization buffer (Fig. S7b in Supporting Information). Compared with the fast migration of three single-stranded nucleic acids (lanes 1—3), the two-component mixture individually showed one band at shorter electrophoresis distance (lanes 4 and 5), indicating the occurrence of partial hybridization between DNA1 and miRNA-21 and between DNA2 and miRNA-21. After the sandwich hybridization among DNA1, DNA2 and miRNA-21, a band with slowest migration rate was observed (lane 6). Upon the sandwich hybridization, TR-FRET occurred from PLNP to FITC, which could be used to sensitively detect miRNA-21. For TRF measurements, DNA1-PLNPs were incubated with target miRNA-21 and FITC-labeled DNA2 (10 nM, Fig. 5a) at the optimal incubation time of 2 h (Fig. 5b). The TR-FRET signal of FITC at 520 nm increased, and the emission intensity of PLNPs at 468 nm obviously reduced as miRNA-21 concentration increased (Fig. 5c), which was attributed to the occurrence of energy transfer from long-lived PLNPs to short-lifetime FITC. This sensing strategy displayed a linear range from 1.0 pM to 1.0 μM with a detection limit of 0.26 pM for miRNA (inset in Fig. 5c). In addition, the PL decay of DNA1-PLNPs at 468 nm was accelerated with the increasing miRNA-21 concentration (Fig. 5d), further confirming the TR-FRET procedure in the presence of miRNA-21.

Alternatively, PDGF is an important protein for cell transformation and tumor growth and progression [55]. For the analysis of PDGF protein, one interesting example is the use of fluorophore-labeled aptamer because of the specific molecular recognition [56]. In this study, PDGF detection was achieved using FITC-aptamer functionalized PLNPs as the nanoprobe (aptamer-PLNPs), which was also characterized by UV—vis spectroscopy (Fig. S7a in Supporting Information). Due to a relatively long distance between PLNP and FITC labeled to the aptamer, the nanoprobe showed a weak TR-FRET signal of FITC at 520 nm. After the aptamer specifically recognized PDGF with a structure switching and thus the FITC was close to the PLNP, the TR-FRET signal enhanced and the emission of PLNPs obviously reduced with the increasing PDGF concentration (Fig. 5f), under the optimal incubation time of 1 h (Fig. 5e). This could be defined as an "on—on" change. Correspondingly, the PL decay of aptamer-PLNPs at 468 nm was accelerated upon addition of PDGF (Fig. 5g). This sensing method showed a linear range from 10 pM to 100 nM with a detection limit of 2.57 pM for PDGF at 3σ (inset in Fig. 5f).

The specificity of the designed methods for the corresponding targets was examined individually. For DNA1-PLNPs, the signal of perfectly complementary target was 3.8 times of that for single-base mismatched oligonucleotide, and the response to three-base mismatched strand was only 4.0% of that to perfectly complementary target (Fig. 5h). The signal of the mutated miRNAs was hardly detectable at the same concentrations with target miRNA-21 of 1 μM or even at that of 10 times (Fig. S8 in Supporting Information), suggesting little effect on the practical application. In the case of PDGF detection, the response of aptamer-PLNPs to the target was at least 4.2 times higher than that to interferants even when their concentrations were 100 times the target (Fig. 5i). Meanwhile, the TRF response of PDGF control DNA-functionalized PLNPs to PDGF was as low as that of the blank (inset in Fig. 5i), suggesting the high specificity of the aptamer-PLNPs for promising application in complex samples.

Table 1
FRET parameters for different PLNP-based conjugates.

Conjugates	Separation distance *r* (nm)	FRET efficiency *E* (%)
Peptide-PLNP	2.8	32.3
DNA1-PLNP	2.9	29.1
Aptamer-PLNP	8.1	0.10

Peptide, DNA1 and Aptamer were all functionalized with FITC as acceptor. Förster radius R_0 was calculated to be 2.5 nm.

3.4. Fluorescence lifetime monitoring of intracellular caspase-3

More importantly, TR-FRET has been identified with the fluorescence lifetime change of the probe upon recognition to the target. Thus fluorescence lifetime imaging of **P1** can be used for monitoring of intracellular caspase-3 activity. Firstly, the

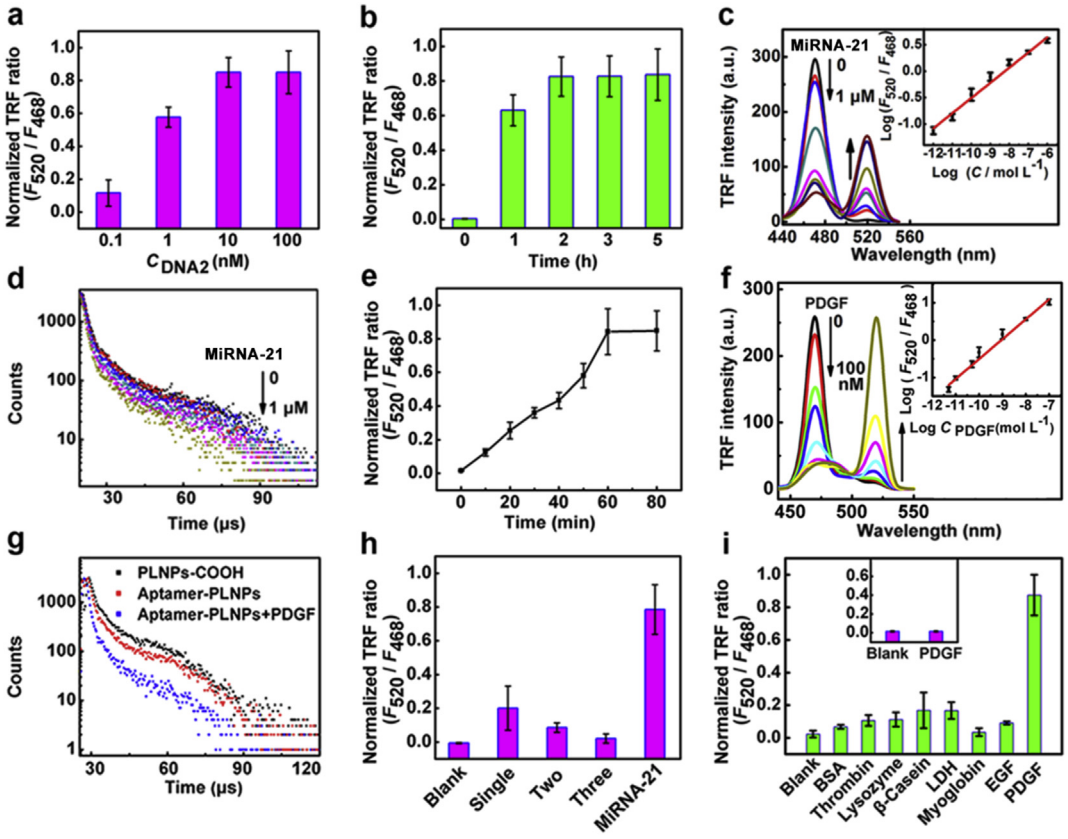

Fig. 5. (a) Dependence of TRF ratio of DNA1-PLNPs (1.0 mg mL^{-1}) and miRNA-21 (1.0 μM) on DNA2 concentration after incubation for 2 h. (b) Effect of incubation time on TRF ratio of DNA1-PLNPs (1.0 mg mL^{-1}), miRNA-21 (1.0 μM) and DNA2 (10 nM). (c) TRF spectra of DNA1-PLNPs (1.0 mg mL^{-1}), DNA2 (10 nM) and miRNA-21 at 0, 1.0 pM, 10 pM, 100 pM, 1.0 nM, 10 nM, 100 nM and 1.0 μM (from top to bottom at 468 nm) after incubation for 2 h. Inset: plot of logarithmic value of TRF ratio *vs*. logarithmic value of miRNA-21 concentration. (d) PL decays at 468 nm after incubating DNA1-PLNPs (1.0 mg mL^{-1}) with DNA2 (10 nM) and miRNA-21 at 0, 100 pM, 1.0 nM, 10 nM, 100 nM and 1.0 μM (from top to bottom) for 2 h. (e) Dependence of TRF ratio of aptamer-PLNPs (1.0 mg mL^{-1}) with PDGF (1.0 nM) on incubation time. (f) TRF spectra of aptamer-PLNPs (1.0 mg mL^{-1}) with PDGF at 0, 5.0 pM, 10 pM, 50 pM, 0.1 nM, 1.0 nM, 10 nM and 100 nM (from top to bottom at 468 nm). Inset: plot of logarithmic value of TRF ratio *vs*. logarithmic value of PDGF concentration. (g) PL decays at 468 nm for PLNPs-COOH (1.0 mg mL^{-1}), aptamer-PLNPs (1.0 mg mL^{-1}), and aptamer-PLNPs + 1.0 nM PDGF. (h) Specificity of DNA1-PLNPs (1.0 mg mL^{-1}) to target miRNA-21 (1.0 μM) and single/two/three base mismatched RNAs (100 μM). (i) Specificity of aptamer-PLNPs (1.0 mg mL^{-1}) to PDGF (1.0 nM) and other interferants (100 nM). Inset: response of PDGF control DNA-functionalized PLNPs (1.0 mg mL^{-1}) to 100 nM PDGF. Blank in h and i is the response of the functionalized PLNPs in the absence of targets. Data represent mean values ± standard deviation, $n = 3$.

cytotoxicity of **P1** was examined with MTT assay. After incubated with **P1** for 10 h, HeLa cells still maintained about 86.6% of the cell viability. Although the doped rare earth metal ions were potentially cytotoxicity, the functionalized PNLPs with biocompatible peptides demonstrated low cytotoxicity of **P1** (Fig. S9 in Supporting Information). Based on the high affinity of cRGD to the $\alpha_v\beta_3$ integrin receptor [57], **P1** could enter HeLa cells via RGD receptor-mediated endocytosis to be accumulated in cytoplasm (Fig. 6a). For subcellular localization of the probe, the confocal microscopic images were taken, which showed that the spot of **P1** was overlapped with the lysosomal tracker, LysoTracker Red (Fig. 6b and c). The calculated Pearson coefficient value of 0.946 indicated reliable co-localization of **P1** with LysoTracker Red and the distribution of **P1** in lysosome after internalization.

To achieve the change of intracellular caspase-3 activity, HeLa cells were treated with cisplatin, a commonly used apoptosis inducer. With the increasing treatment time, the apoptosis percentage obviously increased by the flow cytometric analysis (Fig. 7a), and the caspase-3 activity in cell extract increased and tended to a maximum at a treatment time of 3 h (Fig. 7b). Thus fluorescence lifetime monitoring of intracellular caspase-3 activity could be performed by incubating HeLa cells with **P1** at 37 °C for 4 h, and then apoptosis inducer for different times.

With the increasing incubation time of apoptosis inducer, the cells gradually showed a reddish FLIM images along with the increasing degree of apoptosis (Fig. 8a), which indicated the fluorescence lifetime of **P1** incubated with HeLa cells at 450–495 nm was prolonged and could sense intracellular caspase-3 activity. Cell apoptosis was demonstrated using the apoptosis kit with the dual fluorescence of Annexin V-FITC/PI on a flow cytometric assay in Fig. 7a. The quadrantal distribution of the dual dyes also verified the caspase-dependent early apoptosis. In contrast, the **P2** and then apoptosis inducer-treated HeLa cells did not give appreciable change in the fluorescence lifetime images, even if the increasing degree of apoptosis was obvious from the bright-field images (Fig. 8b). Interestingly, the signal change observed from FLIM was more sensitive than that from confocal fluorescence imaging (Fig. S10 in Supporting Information). This further demonstrated the advantages of FLIM with the long-lived probe in efficiently suppressing the interference of auto-fluorescence from cells [58].

To further demonstrate the fluorescence lifetime change of **P1** during cell apoptosis, the FLIM of treated HeLa cells was investigated in the gray mode with different delay times (Fig. 9). The corresponding lifetimes of **P1**-treated HeLa cells could be calculated from the FLIM without delay to be 460.9, 562.1, 784.2, 1005.4 and 1596.5 ns when the cells were treated with apoptosis inducer

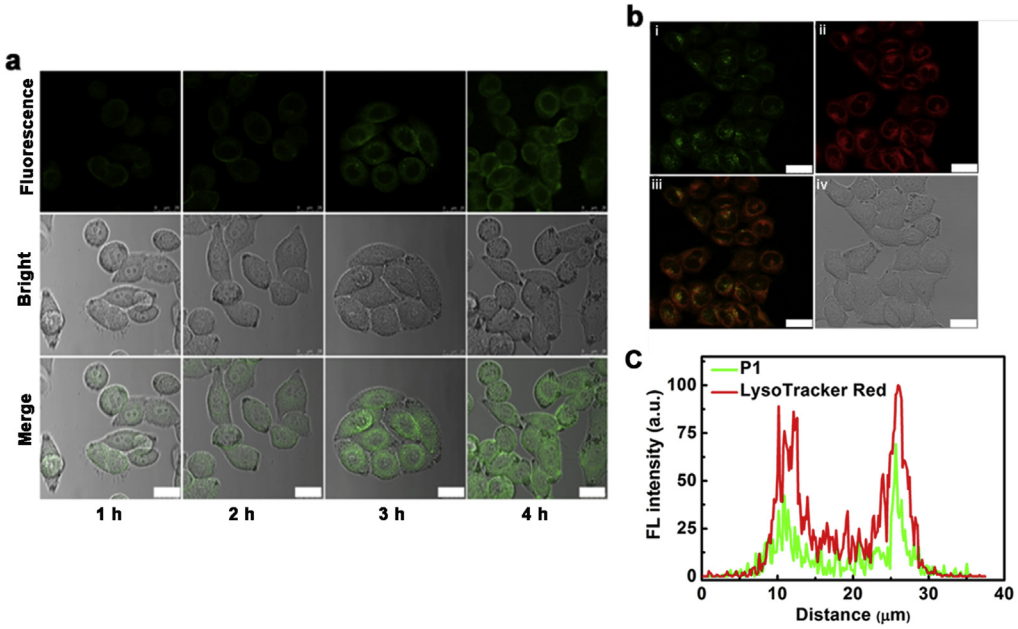

Fig. 6. (a) HeLa cells were incubated with **P1** (0.4 mg mL^{-1}) for different times. (b) HeLa cells were stained with (i) **P1** (1.0 mg mL^{-1}), (ii) LysoTracker Red (50 nM) and (iii) the merge. (iv) The corresponding bright-field image of HeLa cells. Scale bars: 25 μm. (c) Intensity correlation plots of **P1** and LysoTracker Red. (For interpretation of the references to color in this figure legend, the reader is referred to the web version of this article.)

for 0, 0.5, 1, 2 and 3 h, respectively (Figs. 8a and 9a). Setting a delay time of 250.0 ns, the HeLa cells at different treated times showed bright lifetime images (Fig. 9b), while the cells without treatment with apoptosis inducer (0 h) did not show any signal at a delay time of 460.9 ns (Fig. 9c). This appearance was also observed at the delay times of 562.1, 784.2 and 1005.4 ns for the cells treated with apoptosis inducer for 0.5, 1 and 2 h (Fig. 9d–f), respectively, manifesting the responsible lifetimes. Therefore, dynamic lifetime imaging using **P1** could reflect the evolution of cell apoptosis.

To obtain the calibration curve for quantification of intracellular caspase-3 concentration, HeLa cells were first incubated with **P1** for 4 h, and then treated with different amounts of apoptosis inducer for 3 h. The treated cells were conducted on FLIM to obtain the cellular lifetimes (Fig. 10a). Meanwhile, the cell extracts pretreated as above was detected via *in vitro* caspase-3 fluorescent kit to get the fluorescence intensity (Fig. 10b). The corresponding caspase-3 concentration could be calculated by using a linear relationship of fluorescence intensity *vs.* logarithmic value of caspase-3 standard concentration (Fig. 10c). Considering the total cell number, a plot of fluorescence lifetime *vs.* logarithmic value of intracellular caspase-3 concentration in single cell was obtained and showed a good linear relationship (Fig. 10d), which indicated that the lifetime obtained from the FLIM could be used for *in situ* quantification of intracellular caspase-3. The caspase-3 concentration in single HeLa cell incubated with **P1** and then 100 μM apoptosis inducer was calculated to be 4.0×10^{-6} unit mL^{-1}, which was in good agreement with 3.8×10^{-6} unit mL^{-1} obtained from *in vitro* TRF detection using the cell extract. Therefore, a lifetime method was achieved for *in situ* quantitative determination of caspase-3 activity in live cells.

4. Conclusion

Bio-functionalized PLNPs were designed as sensitive nanoprobes for detection of biomolecules and cellular fluorescence lifetime imaging on a TR-FRET platform. We have demonstrated three TR-FRET mechanisms for ratiometric TRF detection of label-free targets such as caspase-3, nucleic acids and proteins. Each of

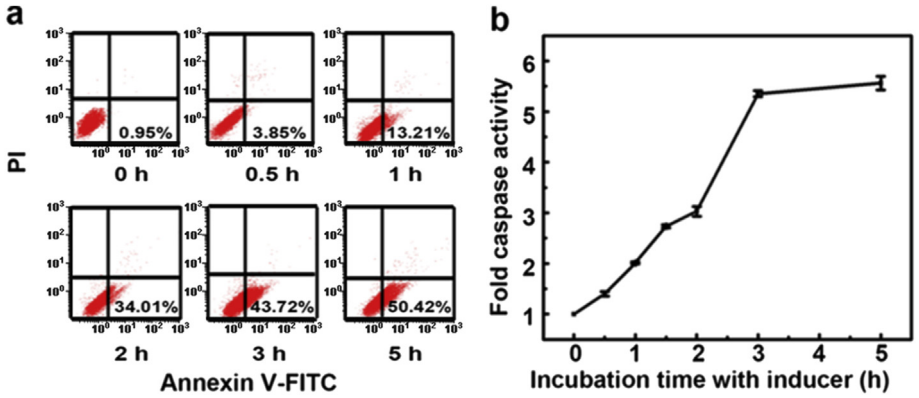

Fig. 7. (a) Flow cytometric analysis of HeLa cells (5.0×10^5) after treated with apoptosis inducer (100 μM) for different times. (b) Time-dependence of caspase-3 activity measured with caspase-3 kit in extracts of HeLa cells (5.0×10^5) treated with apoptosis inducer (100 μM).

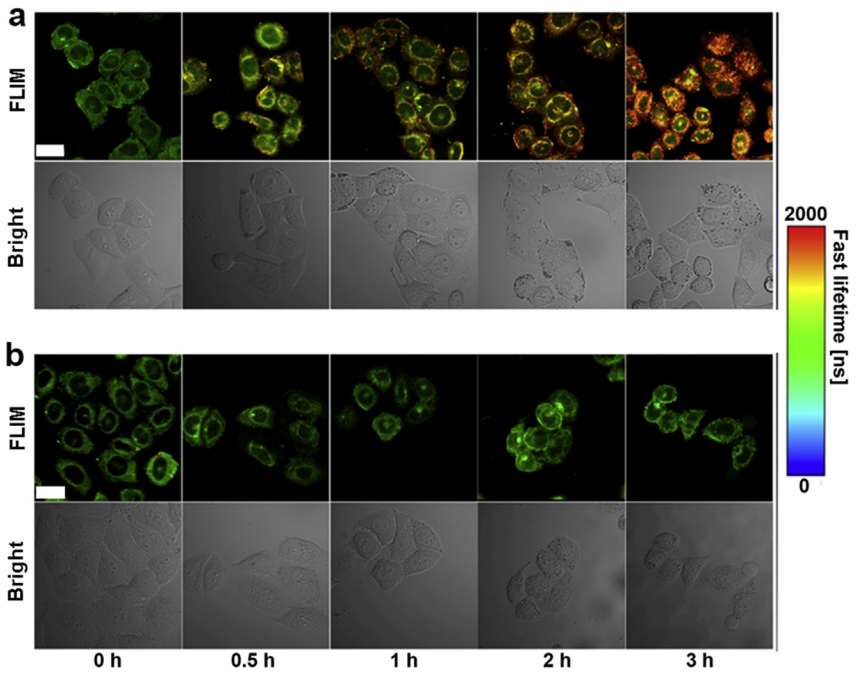

Fig. 8. Fluorescence lifetime images and bright-field images of HeLa cells after incubated with 1.0 mg mL^{-1} (a) **P1** or (b) **P2** for 4 h and then apoptosis inducer (100 μM) for different times. Scale bars: 30 μm.

the approaches shows a wide linear detection range and a low detection limit, indicating the promising potential of the PLNPs-based TR-FRET technique in versatile bioapplications. The evolution of fluorescence lifetime in TR-FRET is also efficiently utilized for monitoring of caspase-3 during cell apoptosis via FLIM. A lifetime method has been established for *in situ* quantification of intracellular caspase-3 activity. PLNPs-based TR-FRET technique not only opens a new perspective for designing sensitive detection methods but also provides a significant tool for dynamically tracking the change of biomolecules *in vivo*.

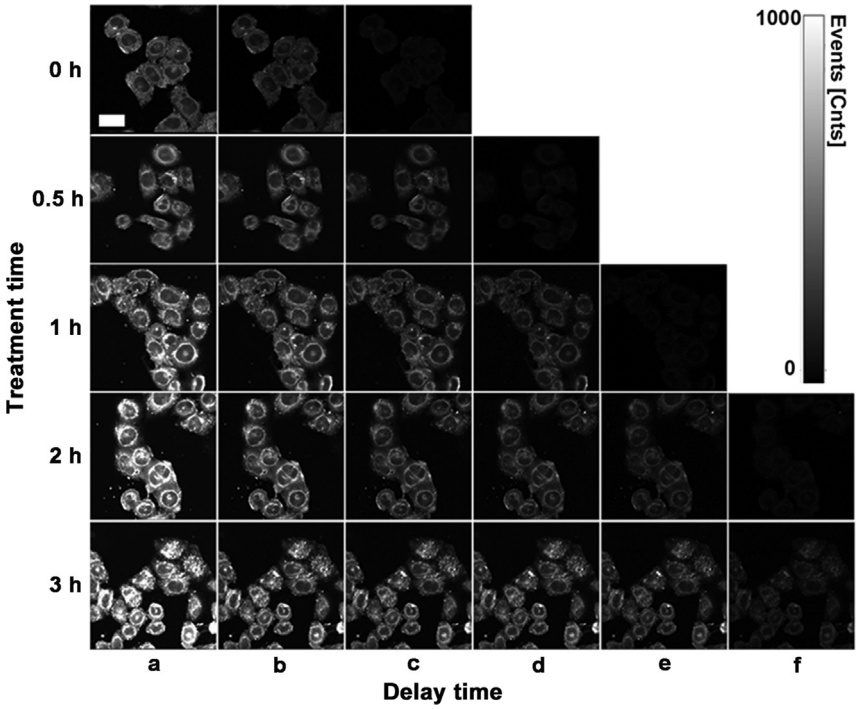

Fig. 9. Fluorescence lifetime images in gray mode for HeLa cells after incubated with **P1** (1.0 mg mL^{-1}) for 4 h and then apoptosis inducer (100 μM) for (a, b, c) 0, 0.5, 1, 2 and 3 h (from top to bottom) at the delay time of (a) 0, (b) 250.0 and (c) 460.9 ns, (d) 0.5, 1, 2 and 3 h (from top to bottom) at the delay time of 562.1 ns, (e) 1, 2 and 3 h (from top to bottom) at the delay time of 784.2 ns, and (f) 2 and 3 h (from top to bottom) at the delay time of 1005.4 ns. Scale bar: 30 μm.

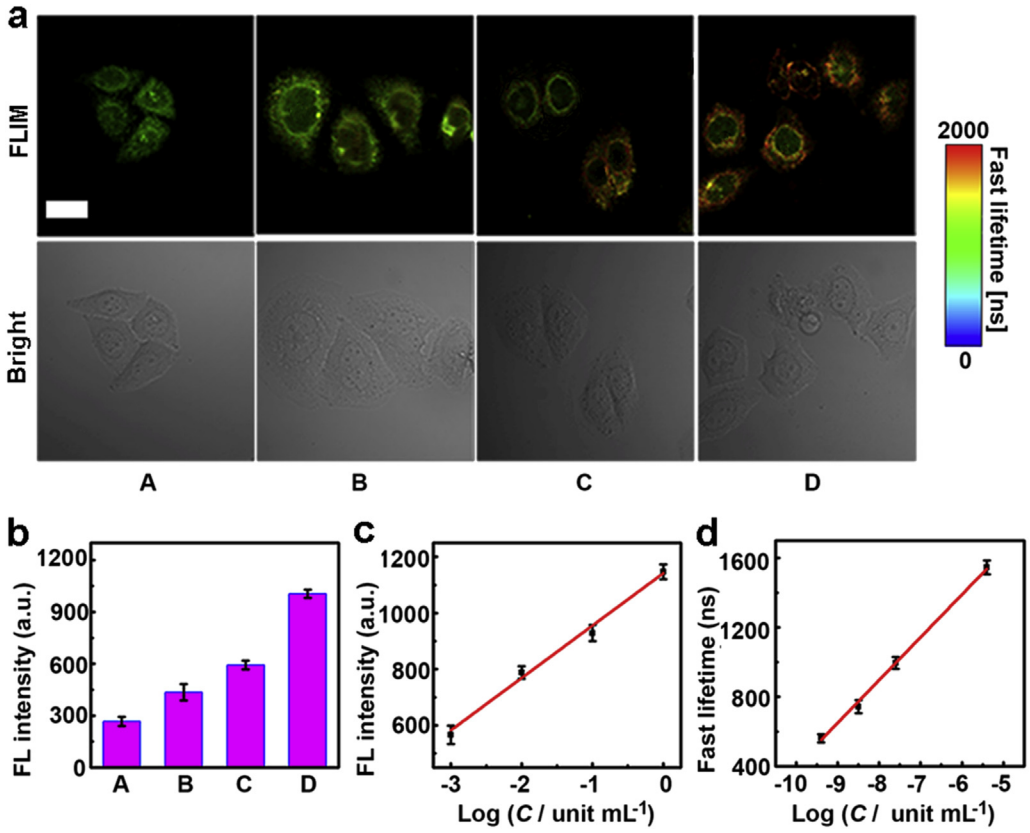

Fig. 10. (a) Fluorescence lifetime images of HeLa cells incubated with **P1** (1.0 mg mL^{-1}) for 4 h and then apoptosis inducer at 12.5, 25.0, 50.0, and 100 μM (from A to D) for 3 h. (b) Fluorescence intensity at 535 nm under the excitation of 485 nm using caspase-3 fluorogenic kit for extracts of HeLa cells incubated with **P1** (1.0 mg mL^{-1}) for 4 h and then apoptosis inducer at 12.5, 25.0, 50.0 and 100 μM (from A to D) for 3 h. (c) Calibration curve of FL intensity *vs.* logarithmic value of caspase-3 concentration with caspase-3 kit. (d) Plot of cellular lifetime *vs.* logarithmic value of caspase-3 concentration in single HeLa cell incubated with **P1**.

Acknowledgment

This study was supported byNational Natural Science Foundation of China (21375060, 21135002, 21121091) and Priority development areas of The National Research Foundation for the Doctoral Program of Higher Education of China (20130091130005).

Appendix A. Abbreviations

cRGD	cyclic arginine–glycine–aspartic acid peptide
DLS	dynamic light scattering
DMF	N,N-dimethylformamide
EDC	1-ethyl-3-(3-dimethyl-aminopropyl)carbodiimide hydrochloride
FITC	fluorescein isothiocyanate
FLIM	fluorescence lifetime imaging microscopy
FRET	fluorescence resonance energy transfer
FT-IR	Fourier transform infrared
HEPES	4-(2-hydroxyethyl)-1-piperazineethanesulfonic acid
MTT	3-(4,5-dimethylthiazol-2-yl)-2-diphenyltetrazolium bromide
PBS	phosphate buffer saline
PDGF	platelet-derived growth factor
PI	propidium iodide
PL	photoluminescence
PLNPs	persistent luminescence nanoparticles
SulfoNHS	N-hydroxysulfosuccinimide sodium salt
TEM	transmission electron microscopic
TEOS	tetraethyl orthosilicate
TGA	thermal gravimetric analyzer
TRF	time-resolved fluorescence
TR-FRET	time-resolved fluorescence resonance energy transfer
Tris	tris(hydroxymethyl)aminomethane
XRD	X-ray powder diffraction

Appendix A. Supplementary data

Supplementary data related to this article can be found at http://dx.doi.org/10.1016/j.biomaterials.2015.07.037.

References

[1] D. Maurel, L. Comps-Agrar, C. Brock, M.L. Rives, E. Bourrier, M.A. Ayoub, et al., Cell-surface protein-protein interaction analysis with time-resolved FRET and snap-tag technologies: application to GPCR oligomerization, Nat. Methods 5 (2008) 561–567.
[2] S.H. Kim, J.R. Gunther, J.A. Katze-nellenbogen, Monitoring a coordinated exchange process in a four-component biological interaction system: development of a time-resolved terbium-based one-donor/three-acceptor multicolor FRET system, J. Am. Chem. Soc. 132 (2010) 4685–4692.
[3] H.E. Rajapakse, D.R. Reddy, L.W. Miller, Luminescent terbium protein labels for time-resolved microscopy and screening, Angew. Chem. Int. Ed. 48 (2009) 4990–4992.
[4] Y.S. Liu, S.Y. Zhou, D.T. Tu, Z. Chen, M.D. Huang, H.M. Zhu, et al., Amine-functionalized lanthanide-doped zirconia nanoparticles: optical spectroscopy, time-resolved fluorescence resonance energy transfer biodetection, and targeted imaging, J. Am. Chem. Soc. 134 (2012) 15083–15090.
[5] M.K. Kuimova, G. Yahioglu, J.A. Levitt, K. Suhling, Molecular rotor measures viscosity of live cells via fluorescence lifetime imaging, J. Am. Chem. Soc. 130 (2008) 6672–6673.
[6] M. Tantama, Y.P. Hung, G. Yellen, Imaging intracellular pH in live cells with a genetically encoded red fluorescent protein sensor, J. Am. Chem. Soc. 133 (2011) 10034–10037.

[7] C.D. Harvey, A.G. Ehrhardt, C. Cellurale, H. Zhong, R. Yasuda, R.J. Davis, et al., Genetically encoded fluorescent sensor of ERK activity, Proc. Natl. Acad. Sci. U. S. A. 105 (2008) 19264–19269.

[8] K. Okabe, N. Inada, C. Gota, Y. Harada, T. Funatsu, S. Uchiyama, Intracellular temperature mapping with a fluorescent polymeric thermometer and fluorescence lifetime imaging microscopy, Nat. Commun. 3 (2012) 705.

[9] Q. Ju, D.T. Tu, Y.S. Liu, R.F. Li, H.M. Zhu, J.C. Chen, et al., Amine-functionalized lanthanide-doped $KGdF_4$ nanocrystals as potential optical/magnetic multimodal bioprobes, J. Am. Chem. Soc. 134 (2011) 1323–1330.

[10] Q. Ju, Y.S. Liu, D.T. Tu, H.M. Zhu, R.F. Li, X.Y. Chen, Lanthanide-doped multicolor GdF_3 nanocrystals for time-resolved photoluminescent biodetection, Chem. -Eur. J. 17 (2011) 8549–8554.

[11] Y.S. Liu, D.T. Tu, H.M. Zhu, X.Y. Chen, Lanthanide-doped luminescent nanoprobes: controlled synthesis, optical spectroscopy, and bioapplications, Chem. Soc. Rev. 42 (2013) 6924–6958.

[12] D.T. Tu, L.Q. Liu, Q. Ju, Y.S. Liu, H.M. Zhu, R.F. Li, et al., Time-resolved FRET biosensor based on amine-functionalized lanthanide-doped $NaYF_4$ nanocrystals, Angew. Chem. Int. Ed. 50 (2011) 6306–6310.

[13] W. Zheng, S.Y. Zhou, Z. Chen, P. Hu, Y.S. Liu, D.T. Tu, et al., Sub-10 nm lanthanide-doped CaF_2 nanoprobes for time-resolved luminescent biodetection, Angew. Chem. Int. Ed. 52 (2013) 6671–6676.

[14] M.Y. Berezin, S. Achilefu, Fluorescence lifetime measurements and biological imaging, Chem. Rev. 110 (2010) 2641–2684.

[15] K. Hoffmann, T. Behnke, D. Drescher, J.U. Kneipp, Near-infrared-emitting nanoparticles for lifetime-based multiplexed analysis and imaging of living cells, ACS Nano 7 (2013) 6674–6684.

[16] L. Gu, D.J. Hall, Z. Qin, E. Anglin, J. Joo, D.J. Mooney, et al., In vivo time-gated fluorescence imaging with biodegradable luminescent porous silicon nanoparticles, Nat. Commun. 4 (2013) 2326.

[17] A. Orte, J.M. Alvarez-Pez, M.J. Ruedas-Rama, Fluorescence lifetime imaging microscopy for the detection of intracellular pH with quantum dot nanosensors, ACS Nano 7 (2013) 6387–6395.

[18] A. Abdukayum, J.T. Chen, Q. Zhao, X.P. Yan, Functional near infrared-emitting Cr^{3+}/Pr^{3+} co-doped zinc allogermanate persistent luminescent nanoparticles with superlong afterglow for in vivo targeted bioimaging, J. Am. Chem. Soc. 135 (2013) 14125–14133.

[19] A.S. Paterson, B. Raja, G. Garvey, A. Kolhatkar, A.E.V. Hagström, K. Kourentzi, et al., Anal. Chem. 86 (2014) 9481–9488.

[20] A. Abdukayum, C.X. Yang, Q. Zhao, J.T. Chen, L.X. Dong, X.P. Yan, Gadolinium complexes functionalized persistent luminescent nanoparticles as a multimodal probe for near-infrared luminescence and magnetic resonance imaging in vivo, Anal. Chem. 86 (2014) 4096–4101.

[21] M. Allix, S. Chenu, E. Véron, T. Poumeyrol, E.A. Kouadri-Boudjelthia, S. Alahraché, et al., Considerable improvement of long-persistent luminescence in germanium and tin substituted $ZnGa_2O_4$, Chem. Mater. 25 (2013) 1600–1606.

[22] Z. Pan, Y.Y. Lu, F. Liu, Sunlight-activated long-persistent luminescence in the near-infrared from Cr^{3+}-doped zinc gallogermanates, Nat. Mater. 11 (2012) 58–63.

[23] B.Y. Wu, X.P. Yan, Bioconjugated persistent luminescence nanoparticles for Föster resonance energy transfer immunoassay of prostate specific antigen in serum and cell extracts without in situ excitation, Chem. Commun. 51 (2015) 3903–3906.

[24] Q. Masne de Chermont, C. Chanéac, J. Seguin, F. Pelle, S. Maîtrejean, J.P. Jolivet, et al., Nanoprobes with near-infrared persistent luminescence for in vivo imaging, Proc. Natl. Acad. Sci. U. S. A. 104 (2007) 9266–9271.

[25] T. Maldiney, C. Richard, J. Seguin, N. Wattier, M. Bessodes, D. Scherman, Effect of core diameter, surface coating, and PEG chain length on the biodistribution of persistent luminescence nanoparticles in mice, ACS Nano 5 (2011) 854–862.

[26] T. Maldiney, A. Bessière, J. Seguin, E. Teston, S.K. Sharma, B. Viana, et al., The in vivo activity of persistent nanophosphors for optical imaging of vascularization, tumors and grafted cells, Nat. Mater. 13 (2014) 418–426.

[27] T. Maldiney, A. Lecointre, B. Viana, A. Bessière, M. Bessodes, D. Gourier, et al., Controlling electron trap depth to enhance optical properties of persistent luminescence nanoparticles for in vivo imaging, J. Am. Chem. Soc. 133 (2011) 11810–11815.

[28] N. Li, W. Diao, Y.Y. Han, W. Pan, T.T. Zhang, B. Tang, MnO_2-modified persistent luminescence nanoparticles for detection and imaging of glutathione in living cells and in vivo, Chem. -Eur. J. 20 (2014) 16488–16491.

[29] B.Y. Wu, H.F. Wang, J.T. Chen, X.P. Yan, Fluorescence resonance energy transfer inhibition assay for α-fetoprotein excreted during cancer cell growth using functionalized persistent luminescence nanoparticles, J. Am. Chem. Soc. 133 (2010) 686–688.

[30] Y.R. Tang, H.J. Song, Y.Y. Su, Y. Lv, Turn-on persistent luminescence probe based on graphitic carbon nitride for imaging detection of biothiols in biological fluids, Anal. Chem. 85 (2013) 11876–11884.

[31] N. Li, Y.H. Li, Y.Y. Han, W. Pan, T.T. Zhang, B. Tang, A highly selective and instantaneous nanoprobe for detection and imaging of ascorbic acid in living cells and in vivo, Anal. Chem. 6 (2014) 3924–3930.

[32] A.P. Savitsky, A.L. Rusanov, V.V. Zherdeva, T.V. Gorodnicheva, M.G. Khrenova, FLIM-FRET imaging of caspase-3 activity in live cells using pair of red fluorescent proteins, Theranostics 2 (2012) 215–226.

[33] W.H. Kong, D.K. Sung, K.S. Kim, H.S. Jung, E.J. Gho, S.H. Yun, et al., Self-assembled complex of probe peptide-*E. coli* RNA I conjugate and nano graphene oxide for apoptosis diagnosis, Biomaterials 33 (2012) 7556–7564.

[34] J. Vuojola, M. Syrjänpää, U. Lamminmäki, T. Soukka, Genetically encoded protease substrate based on lanthanide-binding peptide for time-gated fluorescence detection, Anal. Chem. 85 (2012) 1367–1373.

[35] H.B. Wang, Q. Zhang, X. Chu, T.T. Chen, J. Ge, R.Q. Yu, Graphene oxide–peptide conjugate as an intracellular protease sensor for caspase-3 activation imaging in live cells, Angew. Chem. Int. Ed. 50 (2011) 7065–7069.

[36] H.B. Shi, R.T.K. Kwok, J.Z. Liu, B.G. Xing, B.Z. Tang, B. Liu, Real-time monitoring of cell apoptosis and drug screening using fluorescent light-up probe with aggregation-induced emission characteristics, J. Am. Chem. Soc. 134 (2012) 17972–17981.

[37] J. Zhang, X. Wang, W.J. Cui, W.W. Wang, H.M. Zhang, L. Liu, et al., Visualization of caspase-3-like activity in cells using a genetically encoded fluorescent biosensor activated by protein cleavage, Nat. Commun. 4 (2013) 2157.

[38] D.J. Ye, A.J. Shuhendler, L.N. Cui, L. Tong, S.S. Tee, G. Tikhomirov, et al., Bioorthogonal cyclization-mediated in situ self-assembly of small molecule probes for imaging caspase activity in vivo, Nat. Chem. 6 (2014) 519–526.

[39] X.L. Huang, M. Swierczewska, K.Y. Choi, L. Zhu, A. Bhirde, J. Park, et al., Multiplex imaging of an intracellular proteolytic cascade by using a broad-spectrum nanoquencher, Angew. Chem. Int. Ed. 51 (2012) 1625–1630.

[40] N.P. Damayanti, L.L. Parker, J.M.K. Irudayaraj, Fluorescence lifetime imaging of biosensor peptide phosphorylation in single live cells, Angew. Chem. Int. Ed. 52 (2013) 3931–3934.

[41] T. Maldiney, G. Byk, N. Wattier, J. Seguin, R. Khandadash, M. Bessodes, et al., Synthesis and functionalization of persistent luminescence nanoparticles with small molecules and evaluation of their targeting ability, Int. J. Pharm. 423 (2012) 102–107.

[42] T. Maldiney, M.U. Kaikkonen, J. Seguin, Q. le Masne de Chermont, M. Bessodes, K.J. Airenne, et al., In vitro targeting of avidin-expressing glioma cells with biotinylated persistent luminescence nanoparticles, Bioconjugate Chem. 23 (2012) 472–478.

[43] A.R. Clapp, I.L. Medintz, J.M. Mauro, B.R. Fisher, M.G. Bawendi, H. Mattoussi, Fluorescence resonance energy transfer between quantum dot donors and dye-labeled protein acceptors, J. Am. Chem. Soc. 126 (2003) 301–310.

[44] M.C. Chirio-Lebrun, M. Prats, Fluorescence resonance energy transfer (FRET): theory and experiments, Biochem. Educ. 26 (1998) 320–323.

[45] G.A. Crosby, J.N. Demas, Measurement of photoluminescence quantum yields, J. Phys. Chem. 75 (1971) 991–1024.

[46] I.L. Medintz, A.R. Clapp, H. Mattoussi, E.R. Goldman, B. Fisher, J.M. Mauro, Self-assembled nanoscale biosensors based on quantum dot FRET donors, Nat. Mater. 2 (2003) 630–638.

[47] Q. Fei, C.K. Chang, D.L. Mao, Luminescent properties of $Sr_2MgSi_2O_7$ and $Ca_2MgSi_2O_7$ long lasting phosphors activated by Eu^{2+}, Dy^{3+}, J. Alloys Compd. 390 (2005) 133–137.

[48] X.W. Yan, L.M. Yang, Q.Q. Wang, Lanthanide-coded protease-specific peptide–nanoparticle probes for a label-free multiplex protease assay using element mass spectrometry: a proof-of-concept study, Angew. Chem. Int. Ed. 50 (2011) 5130–5133.

[49] K. Boeneman, B.C. Mei, A.M. Dennis, G. Bao, J.R. Deschamps, H. Mattoussi, et al., Sensing caspase 3 activity with quantum dot-fluorescent protein assemblies, J. Am. Chem. Soc. 131 (2009) 3828–3829.

[50] D.E. Prasuhn, A. Feltz, J.B. Blanco-Canosa, K. Susumu, M.H. Stewart, B.C. Mei, et al., Quantum dot peptide biosensors for monitoring caspase 3 proteolysis and calcium ions, ACS Nano 4 (2010) 5487–5497.

[51] I.L. Medintz, A.R. Clapp, F.M. Brunel, T. Tiefenbrunn, H.T. Uyeda, E. Chang, et al., Proteolytic activity monitored by fluorescence resonance energy transfer through quantum-dot–peptide conjugates, Nat. Mater. 5 (2006) 581–589.

[52] J. Karvinen, V. Laitala, M.L. Mäkinen, O. Mulari, J. Tamminen, J. Hermonen, et al., Fluorescence quenching-based assays for hydrolyzing enzymes. Application of time-resolved fluorometry in assays for caspase, helicase, and phosphatase, Anal. Chem. 76 (2004) 1429–1436.

[53] W. Gao, L.F. Ji, L. Li, G.W. Cui, K.H. Xu, P. Li, et al., Bifunctional combined Au–Fe_2O_3 nanoparticles for induction of cancer cell-specific apoptosis and real-time imaging, Biomaterials 33 (2012) 3710–3718.

[54] A. Keller, P. Leidinger, A. Bauer, A. Elsharawy, J. Haas, C. Backes, et al., Toward the blood-borne mirnome of human diseases, Nat. Methods 8 (2011) 841–843.

[55] J. Yu, C. Ustach, H.R.C. Kim, Platelet-derived growth factor signaling and human cancer, J. Biochem. Mol. Biol. 36 (2003) 49–59.

[56] C.C. Huang, C.K. Chiang, Z.H. Lin, K.H. Lee, H.T. Chang, Bioconjugated gold nanodots and nanoparticles for protein assays based on photoluminescence quenching, Anal. Chem. 80 (2008) 1497–1504.

[57] M.H. Lee, J.Y. Kim, J.H. Han, S. Bhuniya, J.L. Sessler, C. Kang, et al., Direct fluorescence monitoring of the delivery and cellular uptake of a cancer-targeted RGD peptide-appended naphthalimide theragnostic prodrug, J. Am. Chem. Soc. 134 (2012) 12668–12674.

[58] N.P. Damayanti, L.L. Parker, J.M.K. Irudayaraj, Fluorescence lifetime imaging of biosensor peptide phosphorylation in single live cells, Angew. Chem. Int. Ed. 52 (2013) 3931–3934.